AGU ADVANCING EARTH AND SPACE SCIENCE

JGR Biogeosciences

RESEARCH ARTICLE
10.1029/2020JG005815

Key Points:

- Thinning in a ponderosa pine forest resulted in significant increases to annual tree growth and water uptake into the drought period
- At the stand level, density reductions reduced net primary production by 40%–50% within the 3-years observation period
- Emissions from killed biomass resulted in a modeled terrestrial carbon deficit of ~27 Mg C ha^{-1} relative to control stands through 2050

Supporting Information:

- Supporting Information S1

Correspondence to:
T. W. Hudiburg,
thudiburg@uidaho.edu

Citation:
Stenzel, J. E., Berardi, D. B., Walsh, E. S., & Hudiburg, T. W. (2021). Restoration thinning in a drought-prone Idaho forest creates a persistent carbon deficit. *Journal of Geophysical Research: Biogeosciences*, *126*, e2020JG005815. https://doi.org/10.1029/2020JG005815

Received 30 APR 2020
Accepted 22 JAN 2021

Author Contributions:

Conceptualization: J. E. Stenzel, T. W. Hudiburg
Data curation: D. M. Berardi, E. S. Walsh
Formal analysis: J. E. Stenzel, D. M. Berardi, E. S. Walsh, T. W. Hudiburg
Funding acquisition: T. W. Hudiburg
Investigation: J. E. Stenzel, D. M. Berardi, T. W. Hudiburg
Methodology: J. E. Stenzel, T. W. Hudiburg
Project administration: T. W. Hudiburg
Writing – original draft: J. E. Stenzel, D. M. Berardi, E. S. Walsh, T. W. Hudiburg
Writing – review & editing: D. M. Berardi, E. S. Walsh, T. W. Hudiburg

Restoration Thinning in a Drought-Prone Idaho Forest Creates a Persistent Carbon Deficit

J. E. Stenzel[1], D. M. Berardi[1], E. S. Walsh[1], and T. W. Hudiburg[1]

[1]Department of Forest, Rangeland, and Fire Sciences, University of Idaho, Moscow, ID, USA

Abstract Western US forests represent a carbon sink that contributes to meeting regional and global greenhouse gas targets. Forest thinning is being implemented as a strategy for reducing forest vulnerability to disturbance, including mortality from fire, insects, and drought, as well as protecting human communities. However, the terrestrial carbon balance impacts of thinning remain uncertain across regions, spatiotemporal scales, and treatment types. Continuous and in situ long-term measurements of partial harvest impacts to stand-scale carbon and water cycle dynamics are nonetheless rare. Here, we examine post-thinning carbon and water flux impacts in a young ponderosa pine forest in Northern Idaho. We examine in situ stock and flux impacts during the 3 years after treatment as well as simulate the forest sector carbon balance through 2050, including on and off-site net emissions. During the observation period, increases in tree-scale net primary production (NPP) and water use persistence through summer drought did not overcome the impacts of density reduction, leading to 45% annual reductions of NPP. Growth duration remained constrained by summer drought in control and thinned stands. Ecosystem model and life cycle assessment estimates demonstrated a net forest sector carbon deficit relative to control stands of 27.0 Mg C ha^{-1} in 2050 due to emissions from dead biomass pools despite increases to net ecosystem production. Our results demonstrate dynamics resulting in carbon losses from forest thinning, providing a baseline with which to inform landscape-scale modeling and assess tradeoffs between harvest losses and potential gains from management practices.

1. Introduction

Removal of atmospheric CO_2 by the world's forests is now an essential component of limiting global warming to 1.5°C–2°C in addition to large reductions in fossil fuel emissions (IPCC, 2018). Forests remove atmospheric carbon via photosynthesis, accumulating large quantities of carbon in long-lived, lignin-dominated pools, most notably tree wood and soils. This is particularly evident in regions recovering from historically high levels of harvest (Hudiburg et al., 2019; Law et al., 2018). In the Western US, decreases in net carbon uptake (i.e., net ecosystem production [NEP]) due to drier conditions in water-limited environments and increases in mortality events from fire, insects, and drought (Abatzoglou & Williams, 2016; Allen et al., 2010; Hicke et al., 2012; Schwalm et al., 2012; van der Molen et al., 2011) may decrease global greenhouse gas (GHG) mitigation potential of forests by increasing carbon losses relative to gains. In part due to concerns over declining carbon sink strength in some areas, forest thinning is being explored and implemented as a wide scale mitigation strategy (State of California, 2018), particularly in states with GHG reduction mandates (California, Oregon, Washington). However, in situ observations of thinning impacts on carbon and water dynamics are limited, especially with measurements spanning the important temporal and spatial scales at which these impacts occur (from seconds to years and leaves to landscapes).

Forest thinning has become a common strategy for reducing individual tree stress and potentially decreasing tree mortality (Franklin et al., 2018; Liang et al., 2018; Sohn et al., 2016; U.S. Executive Office of the President, 2018), yet thinning is a management practice with inherent carbon costs because live trees are killed, reducing primary producer density and increasing dead biomass available for decomposition or combustion (both within and outside of the ecosystem) (James et al., 2018; Law et al., 2013). To justify specific removal treatments for carbon storage benefits, the net emissions costs of thinning must be lower than the costs of inaction at the temporal and spatial scales of focus, regardless of an ecosystem's baseline sink or source strength (Hudiburg et al., 2011; Law et al., 2013; Mitchell et al., 2012; Naudts et al., 2016). However, the carbon balance impacts of treatments remain uncertain across tree, ecosystem, and regional scales due to

large variations in ecosystem processes, stochastic landscape disturbances, unclear assessment time scales, variable treatment and accounting methods, and historically unprecedented climate. This complexity precludes a "one size fits all" approach to prescriptions (Brown et al., 2004; DellaSala et al., 2013; Hudiburg et al., 2019; Law et al., 2018). Moreover, sufficient continuous measurements of before and after carbon stocks and fluxes in control and thinned stands are often lacking (Tsamir et al., 2019), especially measurements that can be used to improve and validate the mechanics of the larger scale modeling (M. D. Hurteau et al., 2016; Liang et al., 2018; McCauley et al., 2019) that is essential to evaluating landscape outcomes.

Natural and human disturbances, including fire, insects, drought, and harvest, can reduce NEP through altering the balance between ecosystem gross primary production (GPP, i.e., photosynthesis) and total ecosystem respiration (ER) (Chapin et al., 2006). NEP can be reduced in the absence of tree mortality due to greater sensitivity of GPP than respiration to stressors, as shown from eddy covariance estimates during turn of the 21st century drought in western North America and Europe (Ciais et al., 2005; Schwalm et al., 2010, 2012; Zhao & Running, 2010). Mortality events generate large reductions in net primary production (NPP) (i.e., growth, or GPP minus autotrophic respiration) via decreases in live plant density and pulses of dead biomass decomposition that may last years to centuries (J. L. Campbell et al., 2016; van der Molen et al., 2011). The net ecosystem carbon balance (NECB) represents the total ecosystem carbon balance and includes losses from fire emissions or human removals. In the case of forest fire, direct emissions result from combustion of biomass stocks, but typically account for less than 30% of aboveground carbon, are small in relation to subsequent decomposition after high-severity fire, and are primarily limited to dead biomass on the forest floor (J. Campbell et al., 2007; J. L. Campbell et al., 2016; Harris et al., 2019; Meigs et al., 2009; Stenzel et al., 2019).

In examining disturbance from harvest, however, it is important to recognize that NECB is an ecosystem mass balance and does not account for the net emission of ecosystem-derived carbon to the atmosphere. In other words, "out-of-site" is not "out-of-mind" when accounting for net emissions because all removed biomass eventually decomposes or is combusted (Harmon et al., 1996). The Net Forest Sector Carbon Balance (NSCB; Hudiburg et al., 2019) accounts for net emissions of ecosystem carbon from NEP, on-site combustion, and off-site emissions estimated via life cycle assessment (LCA).

Thinning for disturbance mitigation is intended to generally increase residual tree resistance to stressors, increasing individual tree carbon and water status and decreasing probability of mortality. However, killing live tree biomass can decrease ecosystem carbon storage over baseline conditions on decadal scales (Goetz et al., 2012), with storage losses, time until recovery, and residual tree growth positively correlated with thinning intensity (Zhou et al., 2013). These processes vary regionally and there are few studies that have continuously measured water and carbon fluxes both before and after thinning, measured at stand scales, and included control plots (Dore et al., 2010, 2012). Instead, studies have primarily relied on single or periodic carbon stock inventories and modeling. This is important because modeling studies should be validated against data (measurements) of the process-based responses before quantifying carbon emissions for entire regions.

Thinning can impact forest response to stressors through modifying the availability of water, light, and nutrients to the remaining trees as well as altering microclimates. Particularly in water limited forests, changes to soil water availability and timing can have significant impacts on tree photosynthesis and growth (Tepley et al., 2020). In addition to direct impacts on canopy transpiration, thinning has been shown to result in changes to snowmelt volumes and infiltration through less canopy interception and subsequent sublimation (Krogh et al., 2020; Tague et al., 2019; Varhola et al., 2010). These hydrological changes can change soil water availability via altering the partitioning of evaporation, transpiration, and runoff, most significantly during the spring and summer, when warming temperatures and longer daylengths allow for more substantial photosynthesis in higher latitudes. For forests that experience summer drought, soil water availability in deeper soil layers is also crucial (Brooks et al., 2002) and is affected by the persistence of site snowpack in the spring and timing of snowmelt at higher elevations.

Forest thinning emissions result primarily from the harvest and eventual decomposition or combustion of killed above and belowground biomass. Because harvests differ from natural disturbances in that large quantities of stem biomass are often removed and are emitted off site, conducting a LCA of biomass fates

is critical to estimating carbon emissions, as no biomass is stored indefinitely (Goetz et al., 2012; Hudiburg et al., 2011, 2019). Avoided emissions (e.g., combustion during a subsequent or avoided fire) should also be accounted for, but because fire is stochastic, and will occur in only a fraction of a treated landscape during treatment lifespans, these avoided emissions are difficult to quantify (J. L. Campbell & Ager, 2013). Moreover, the emissions avoided can be less than emissions associated with harvest, depending on the harvest intensity (Berner et al., 2017).

To address the biogeochemical impacts of thinning, we performed a density reduction treatment (thinning) on a ponderosa pine forest in the Northern Rocky Mountains, a region that is underrepresented in long-term forest research networks (e.g., AmeriFlux, LTER, NEON) yet contains some of the most carbon dense forests in the western US. The region is also characterized by seasonal drought stress and forests with high vulnerability to disturbance (Buotte, Law, et al., 2020; Buotte, Levis, et al., 2020). We utilize a novel integration of automated tree and soil measurements, traditional inventory techniques, LCA, and ecosystem modeling to examine response at multiple spatiotemporal scales. Multidecadal ecosystem carbon trajectories in the 21st century are simulated with Daycent (Parton et al., 1998), the daily timestep version of the CENTURY model, to evaluate the consequences of thinning at stand and landscape scales through 2050. Our study addresses the following: What are the impacts of forest thinning on (1) tree-scale carbon and water dynamics, (2) ecosystem scale carbon and water dynamics, and (3) net forest sector carbon balance through 2050? In the short term, we hypothesized that moderate live tree removals would increase individual tree water use and production yet reduce stand carbon uptake due to reductions in live tree density and increases in dead belowground biomass. Moreover, considering the immediate and eventual emissions of biomass removals, we expect that carbon parity with the control stands would take several decades.

2. Materials and Methods

2.1. Study Site Description

The study site is a 35-year old (2015) ponderosa pine (*Pinus ponderosa*) plantation located in the University of Idaho Experimental Forest in Northern Idaho (46.846°N−116.716°W, Figure 1). Pretreatment average basal area was 36 m^2 ha^{-1} and density was 824 trees ha^{-1}. Average tree diameter-at-breast-height (DBH) and height were 23 cm and 15 m. Site elevation is ∼970 m with slopes from 0° to 5° and aspects ranging from ∼135° to 270° southeast to west. The 30-years average annual air temperature and precipitation are 8.3°C and 883 mm, respectively (DayMet; (Thornton, 2012). The previous 40 years mean frost free growing period is 113 days, with every year after 2012 being above average (Hegewisch & Abatzoglou, 2020). Typically, this region experiences prolonged summer drought with consecutive rain free days ranging from 40 to 100 days, resulting in a late-summer drought period in which rooting depth soil moisture is depleted and vapor pressure deficits are high (SNOTEL; Schaefer & Paetzold, 2001). Soils at this location are a silty loam with a volcanic ash layer. Understory shrubs consist of ninebark (*Physocarpus malvaceus*), oceanspray (*Holodiscus dumosus*), and common snowberry (*Symphoricarpus albus*). Understory tree regeneration is largely nonexistent.

2.2. Study Design

Six 0.4-ha (1-acre, 35.7 m radius) plots were installed in the Fall of 2016. In each plot, four subplots (10 m radius) were established following the FAO Terrestrial Carbon Observations protocol (Law et al., 2008), with one subplot in the center and the remaining three 15-m from center in the directions of 0°, 120°, and 240°. Three plots were thinned to 6 m spacing and a 50% reduction in basal area from December 2016 to April 2017, while the remaining three plots remained as control plots. Woody debris and slash from the thinned plots were removed, piled, and burned in accordance with University of Idaho Experimental Forest protocols to prevent fuels build-up and bark beetle habitat. To capture the stand dynamics associated with thinning, we estimated pre and post thinning carbon stocks, carbon fluxes, and water dynamics. We statistically modeled stocks, fluxes, and water dynamics as a function of time, seasonality, and environmental covariates (Tables S2–S4) to identify data patterns and explain intraannual responses. We projected long-term effects of thinning on forest ecosystem carbon balance with a biogeochemical model (DayCent) and life cycle analysis of harvested carbon.

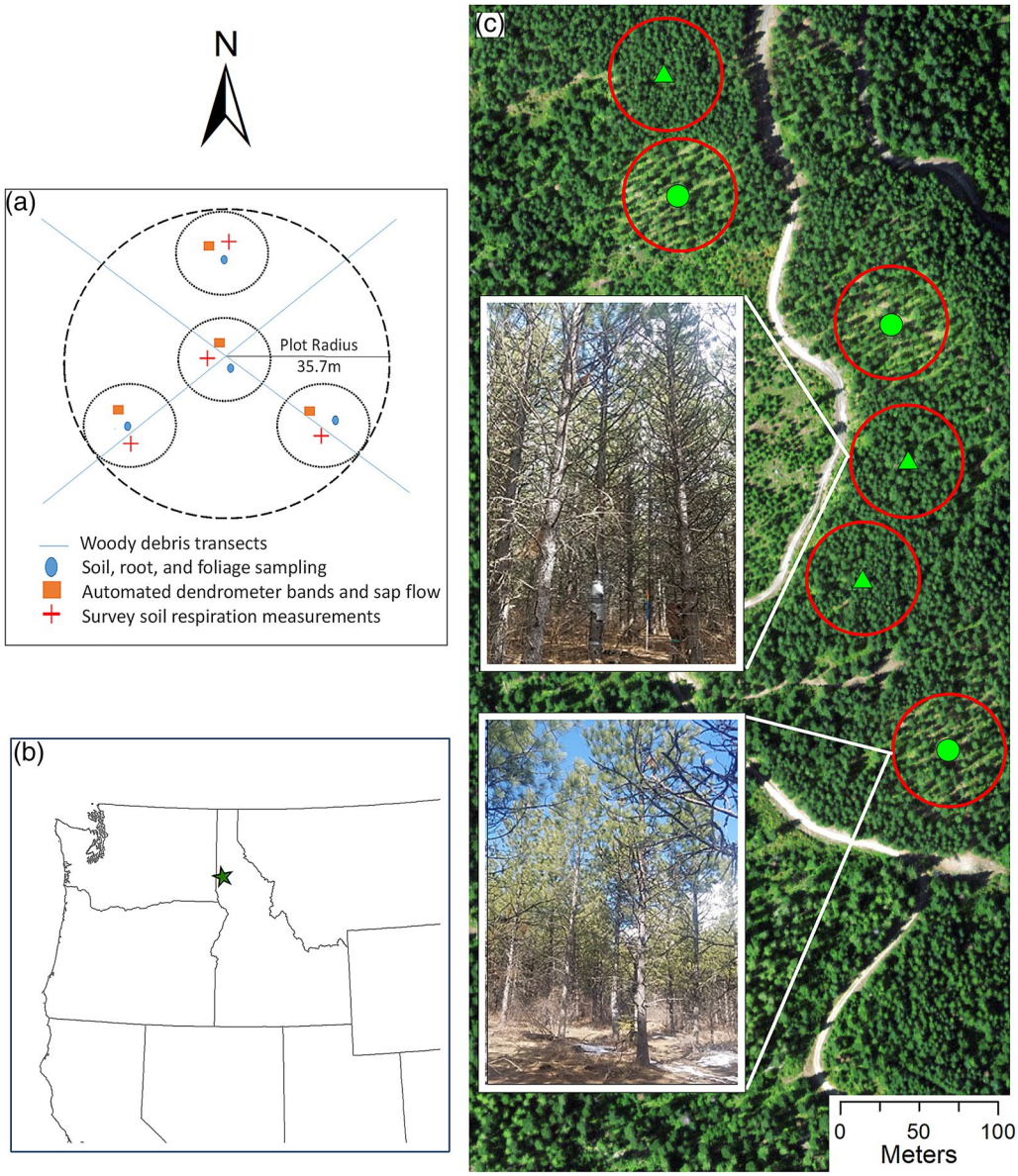

Figure 1. Study location and design. (a) Plot diagram. Locations of sap flow sensors and dendrometers were randomly distributed within 4, 10 m radius subplots. (b) Study location in the Northern Rockies ecoregion near Moscow, ID, USA. (c) Annotated image of study sites within the University of Idaho Experimental Forest, June 2020 (ArcGIS World Imagery, 1.2 m). Red circles indicate plot locations (center circles = thinned, triangles = control). Representative photographs were taken shortly after the thinning treatment in Spring, 2017 (photo credit: T. Hudiburg).

2.3. Carbon Stock and Biometric Measurements

Sampling size and frequency differed for the measured biomass pools (see Table 1). For all biomass pools, conversions to carbon are calculated based on a carbon to biomass ratio of 0.5. Live and dead tree biomass were calculated using regional and species-specific allometric equations that use height and DBH for estimating bole and coarse root volume, bark, branch, fine root, and foliage biomass (Means et al., 1996). Site-specific wood density was used to convert bole and coarse root volume to biomass. Standing dead tree carbon is based on recorded biomass and decay class and reduced over time by standing dead decay rates.

Understory woody shrub biomass was estimated using site-specific allometric equations based on in situ samples of shrubs. We estimated percent cover and height classes for a sample of shrubs, then harvested, dried, and weighed samples to develop the biomass equations. Subsequently, all shrub percent cover and

Table 1
Carbon Stock and Biometric Field Sampling Structure

Inventory	Year	Season	Scale	Samples (*n* per plot)
Tree	2016, 2019	Summer	Subplot	Complete
Understory	2016, 2019	Summer	Subplot	Complete
Woody Debris	2016, 2019	Summer	Plot	A 10-m (fine) and 45-m (coarse) (2)
Soil	2016	Summer	Plot	4 per plot (4)
Litter and Duff	2019	Fall	Plot	4 per plot (4)
Roots	2016, 2017, 2018, 2019	Spring, Fall	Subplot	3 per subplot (12)

height class within each subplot were measured to estimate total shrub biomass of each plot. Thinning operations destroyed over 85% of shrub biomass with negligible re-sprout prior to the 2019 sampling. Herbaceous and grass biomass were negligible in all the plots and not included in our estimates.

Plot level fine and coarse woody debris carbon pools were estimated using line-transects that extended in each cardinal direction from the center of the plots (Law et al., 2008; Van Wagner, 1968), with density modifiers by species and decay class. All stump diameters, heights, species, and decay classes were recorded for each plot. Stump volume was calculated as a cylinder and converted to biomass with a decay-class constant modifier for density.

Soil samples (10 cm^2) were measured for carbon and nitrogen content at 0–5 cm, 5–10 cm, 10–20 cm, and 20–30 cm. Litter and duff were separated from these samples (Chojnacky et al., 2009), dried, and weighed in the laboratory. Field depth of litter and duff was measured and bulk density was calculated; biomass to carbon conversion factors of 0.37 and 0.49, respectively were used to estimate carbon stocks of each (M. Hurteau & North, 2009).

Root biomass cores were collected from the top 20-cm of the soil profile. Roots were separated from the soil, dried, sorted into size classes (<2 mm, 2–5 mm, and >5 mm), and weighed to get seasonal biomass of fine and coarse roots. Root biomass was used to estimate the carbon pool size of roots as well as fine root turnover.

2.4. Carbon and Water Flux Measurements

Automated measurements of soil moisture, soil temperature, sap flow, bole circumference growth, and soil respiration occurred from 2017 to 2019. Primary data collection occurred through the months of March through November and is the focus of analysis.

Meteorological data were captured through a combination of on-site sensors and nearby meteorological stations. On site climate and soil measurements were augmented with precipitation and air temperature from the Moscow Mountain SNOTEL station located on the same ridge as the study site (Schaefer & Paetzold, 2001). Air temperature and relative humidity within the mid-canopy (4.5–6 m) of 1 tree per plot were measured using MicroDAQ LogTag model HAXO-8 humidity and temperature recorders (MicroDAQ.com Ltd., Contoocook, NH, USA). Soil moisture and temperature were measured at half hourly intervals with CS650 sensors (Campbell Scientific, Logan, UT, USA). Probes were placed in the soil, horizontally at 10, 30, and 80 cm in the soil profile in each plot in a location where slope and canopy coverage were representative of the majority of the plot.

Sap flow was measured in seven trees per plot using paired thermal dissipation sap flow probes (Granier et al., 1996) installed to a depth of 2-cm into the sapwood. The upper probe was continuously heated while voltage differential between the two probes was measured at 5-min intervals using CR1000 dataloggers (Campbell Scientific, Logan, UT, USA). Sap flow measurements were reduced to three trees per plot for the winter months (November–March) each year due to solar power limitations. Time series data were cleaned and converted from differential voltage via the TRACC package for R (Ward et al., 2017). A rolling baseline

zero flow was calculated with a zero-flow vapor pressure deficit (VPD) threshold of 0.1 kPa on nights in which this threshold was met for a minimum of 2 h and linearly interpolated for periods of higher VPD.

Stand sap flux ($E_{t;}$ cm d^{-1}) was calculated with additional inputs of stand inventory observations, including tree DBH and sapwood depth. Plot sap flow was calculated as canopy transpiration ($E_{c;}$ cm m^{-2} d^{-1}; at ≥ daily scale) divided by area. Canopy transpiration was calculated as a product of sap flow (cm h^{-1}), sapwood area, and leaf area at daily and greater scales. To account for flow attenuation at depths greater than 2 cm, relative flux by sapwood depth was calculated according to similarly aged ponderosa pine stands (Irvine et al., 2004). We did not find a relationship between tree size and sap flow at 2 cm (the range of DBH in the stands was narrow in the even aged stand). For trees without sensors in each plot, we estimated flow based on average flow rates adjusted by tree-size-specific estimates of sapwood area and flow attenuation across sapwood depth.

Stand canopy conductance (G_c; cm s^{-1}; Equation 1) was calculated from stand sap flow, intracanopy temperature and relative humidity, and stand LAI, and restricted to periods when VPD greater than or equal to 0.6 kPa. (Drake et al., 2011; Ewers et al., 2001):

$$G_C = K_g(T) \times \frac{E_c}{(VPD \times LAI)}, \tag{1}$$

Where T is temperature (Celsius), VPD is vapor pressure deficit (kPa), LAI is stand leaf area index (unitless) and K_g is the conductance coefficient (Drake et al., 2011). Based on Fick's law, carbon uptake can be calculated a function of $G_C$and the leaf-atmosphere CO_2 gradient. We therefore also assessed the degree to which light-saturated leaf CO_2 concentrations (C_i) were conserved in the study stand (Drake et al., 2011; G. Katul et al., 2001). C_i across the growing season was estimated via leaf starch $\delta^{13}C$, which is the ratio of stable isotopes ^{13}C–^{12}C relative to a standard reference and reflects carbon isotope discrimination associated with photosynthesis (Equations 2 and 3; Farquhar et al., 1989). Mid- and upper canopy sunlit needles were collected across plots during the spring and summer drought period of 2018 ($n = 38$) via the shotgun method, reflecting the isotopic composition of recent photosynthate relative to the standard reference. Needles were dried and ground and starch was extracted via methanol/chloroform/water extraction (Wanek et al., 2001), then packaged in tin capsules. Analysis of $\delta^{13}C$ was performed using a coupled elemental analyzer (ECS 4010, Costech Analytical, Valencia, CA) and continuous flow isotope ratio mass spectrometer (Delta PlusXP, Thermo Finnigan, Bremen, Germany), reported relative to VPD. C_i was calculated as:

$$\Delta = \frac{\delta^{13}C_{\text{air}} - \delta^{13}C_{\text{plant}}}{1 + \delta^{13}C_{\text{plant}}}, \tag{2}$$

$$\Delta = a + (b - a) \times \frac{c_i}{c_a}, \tag{3}$$

Where Δ is discrimination relative to air and a and b are the fractionation due to diffusion and carboxylation (4.4 and 27)‰. We assumed a $\delta^{13}C_{\text{air}}$ of −8‰ and that atmospheric CO_2 was a stable 415 ppm during daytime hours (G. G. Katul & Albertson, 1999).

The seasonality of tree growth was determined using self-logging dendrometer bands. TreeHugger automated dendrometer bands (Global Change Solutions, LLC) were installed on sap flow trees in each plot by March of 2017, ~2 months prior to typical growing season initiation. TreeHugger dendrometer bands record bole circumference changes via shifting stylus depression of a soft potentiometer pad. Dendrometer accuracy is ±10 μm and measurement resolution is 6 μm. Prior to installation, outer stem bark was smoothed with a rasp and chisel. Bands were installed at ~2-m in height (above sap flow probes) and appropriate spring tension for proper stylus-potentiometer overlap was verified. Circumference and band/logger temperature were recorded at 30-min intervals by a dedicated logger associated with each band. Band data was analyzed for determining the seasonality (i.e., rate of growth, start and cessation) of bole wood NPP and reconciled with increment core data to determine annual bole wood NPP.

Current and historical estimates of wood NPP were derived from measuring radial growth increments from 20 trees in each plot, including sap flow trees. NPP of woody components is computed from the difference in biomass at two points in time divided by the measurement interval. Previous DBH (calculated from the wood increment cores) and height (modeled using site-specific diameter height equations) for each tree are used to calculate the previous biomass. Foliage NPP was calculated as foliage biomass divide by plot-specific average leaf retention times (Hudiburg et al., 2011). We were unable to detect significant changes in live and dead root biomass pools between spring and fall sampling periods, and therefore could not calculate fine root NPP in our samples. We used the literature reported average fine root turner over time for North American conifers (0.641; Li et al., 2003) multiplied by fine root biomass to determine fine root NPP.

Total soil respiration (R_s; including both autotrophic [R_a] and heterotrophic [R_h] contributions) was were measured using both automated and survey measurements. Shallow 10-cm diameter collars were installed to a depth of 2-cm at each subplot in March of 2017. Automated measurements of R_s were taken hourly using eosFD forced diffusion chambers (Eosense, Nova Scotia, Canada). Two chambers each were installed at two of the thinned plots and one control plot. Automated measurements were primarily used to evaluate and develop diurnal gap filling techniques for the survey data and for winter R_s measurements while the chambers were under snow and the sites were inaccessible.

Survey measurements of R_s were taken weekly from April–early November between 10:00 a.m. and 2:00 p.m. using an EGM-5 SRC portable gas analyzer (PP Systems, Amesbury, MA, USA). Survey measurements were gap-filled to attain daily, weekly, monthly, and annual totals of R_s using linear interpolation (Gomez-Casanovas et al., 2013). Linear interpolation was selected because it outperformed soil temperature and soil moisture based models (Reichstein et al., 2003) when compared to automated data for periods in which automated R_s data were available.

2.5. Biogeochemical Model Description, Evaluation, and Simulations

An updated and improved version of the DayCent ecosystem model (Parton et al., 1998; Stenzel et al., 2019) was implemented to estimate future NEP dynamics postthinning and estimate the NSCB along with a LCA. DayCent is the globally recognized daily timestep version of the biogeochemical model CENTURY, widely used to simulate the effects of climate and disturbance on ecosystem processes including forests worldwide (Bai & Houlton, 2009; Bartowitz et al., 2019; Hartman et al., 2007; Hudiburg et al., 2017). The current version (Stenzel et al., 2019) now includes a standing dead tree pool (i.e., snag pool) because of the important biogeochemical consequences of having standing dead wood versus live wood that dies and immediately becomes downed coarse woody debris.

Required inputs for the model include vegetation cover, daily precipitation and air temperature, surface soil texture, site coordinates (for solar inputs), and disturbance histories. DayCent calculates potential plant growth as a function of water, light, and soil temperature, and limits actual plant growth based on soil nutrient availability. The model includes three soil organic matter (SOM) pools (active, slow, and passive) with different decomposition rates, above- and below-ground litter pools, and a surface microbial pool associated with the decomposing surface litter. Plant material is split into structural and metabolic material as a function of the lignin to nitrogen ratio of the litter. The active pool (microbial) has short turnover times (1–3 months) and the slow SOM pool (more resistant structural plant material) has turnover times ranging from 10 to 50 years depending on the climate. The passive pool includes physically and chemically stabilized SOM with turnover times ranging from 400 to 4,000 years. Model outputs include soil C and N stocks, live and dead biomass, above- and below-ground NPP, heterotrophic respiration, fire emissions, and NEP, defined as the difference between NPP and heterotrophic respiration. While Daycent does not explicitly represent individual trees, it implicitly represents the effects of stand competition, particularly with regards to the availability of mineral nitrogen and soil moisture.

Site simulations were driven with historic (1950–2005) and projected future climate (daily maximum temperature, minimum temperature, and precipitation) through 2050 under RCP 8.5 (Figure S5). Input data was obtained as 4 km statistically downscaled CCSM4 (CMIP5 GCM ensemble member) data from MACAv2-METDATA (https://climate.northwestknowledge.net/MACA/data_csv.php; Abatzoglou & Brown, 2012). MACA is a statistical downscaling method that has been evaluated for local analysis while

retaining a large set of climate variables. Parameterization of point runs was based on species and local observation-based ecophysiological traits (e.g., Leaf retention time, leaf nitrogen concentration, maximum leaf area index) and site and area specific soil characteristics (observations and SSURGO; Abatzoglou & Brown, 2012; NRCS, 2010). Disturbance history was prescribed based on the experimental thinning and most recent recorded clear cut of the stand in the late 20th century. Model evaluation within the observation period was based on comparison with measured live and dead carbon stocks, aboveground NPP, and seasonal soil volumetric water content (Table S6, Figures S3 and S4). For 2018–2019, model VWC r^2 was 0.72 (Figure S3); in particular, the timing of summer soil dry down followed observations and in turn led to model NPP downregulation. From 2008 to 2016, the r^2 of the modeled aboveground live carbon stock was 0.90, reflecting similar model-observation live-tree trajectories following the 20th century clear cut.

In addition to prognostic future NEP, the emissions tradeoffs between thinning losses and potentially enhanced forest resilience to mortality were evaluated with additional disturbance prescriptions. A range of mass mortality scenarios were prescribed for the higher density unthinned stands only. Scenarios were intended to represent stress related mortality events in which most killed live biomass remains on site (e.g., drought, insect, pathogen, and other chronic stress-related mortality), and thus did not include combustion losses. The future timing (2020–2045) and intensity (50%–90%) of a single mass mortality event was varied and compared to an undisturbed control and thinned stand net emissions by 2050 (Table S1).

2.6. Life-Cycle Assessment and Net Forest Sector Carbon Balance

A LCA was employed to account for the storage and emission of killed harvested biomass that was removed from site or combusted on site. Branches and foliage mass from harvested trees were burned as slash on site within 1 year of the thinning. Removed biomass was divided into product pools including wood and paper products with half-lives of 75 and 2.5 years (Dymond, 2012; Skog, 2008; Smith et al., 2006), respectively. Wood waste (i.e., mill wood that does not become a product) is assumed to be burned onsite with energy recapture or to decay within 1 year. Fossil fuel emissions for all harvesting activities and transport to the mill are also included. We define the Net Forest Sector Carbon Balance (NSCB; see Hudiburg et al., 2019) as the net terrestrial balance of carbon within or derived from the forest ecosystem (NEP—Fire Emissions—wood product chain emission; Table S5). In comparison to NECB (NEP—Fire Emissions—Harvested Biomass), NSCB accounts for net vertical transfers of carbon between the atmosphere and land, delaying the subtraction of removed carbon until it is combusted or decomposes at the end of the product chain lifespan. NEP was modeled with the Daycent ecosystem model, and included decomposition of stumps, course roots, and fine roots killed during harvest.

2.7. Statistical Analyses

Flux differences (except stand scale NPP) between treatments were evaluated using generalized linear mixed-effects tree models (GLMM Tree; Fokkema et al., 2018). These models estimate a global random effects model, recursively partition the data with respect to a set of covariates using model-based recursive partitioning (MOB; Zeileis et al., 2008), and apply localized linear mixed-effects models (LMM; Bates et al., 2014) to partitioned data, that is, MOB terminal nodes. Global linear mixed-effects models did not describe the data well (except for stand scale NPP), partly because of the nonlinear nature of response variables within years. The MOB aided in identification of treatment-subgroups, which was beneficial for non-arbitrary data partitioning into temporally similar responses and improving LMM covariate fitting. Stand scale NPP was modeled for all nontreatment plots for the period 2008–2018 to detect effects of climate without treatment effects. An LMM without the MOB modeling was fit to these data after the MOB model failed to detect subgroupings on the partitioning covariates. Model selection for each flux was based on nested covariate models and assessment of AIC, BIC, and interpretation of model fit. Covariate significance within the selected LMM models was determined using 95% confidence intervals. The nested set of covariates with respect to the fixed effects, random effects, and the MOB models differed among the fluxes (Tables S2–S4). R was used for data analysis, with the glmertree package used for estimation of the GLMM Tree (Fokkema et al., 2018) and the lme4 package used for the LMM.

Table 2
Average Plot-Level Pre and Postthinned Carbon Pools and NPP

	Total tree (live and dead)	Woody debris	Understory vegetation	Litter/Duff	Soil	Total ecosystem carbon	NPP
2012–2016							
Control	102.2 (3.9)	33.1 (1.6)	5.4 (0.2)	16.2 (3.8)	56.1 (8.4)	213.1 (13.1)	784.9 (84.8)
Thinned	101.6 (15.9)	34.8 (4.6)	5.5 (0.8)	16.9 (6.7)	51.4 (8.4)	210.2 (19.3)	794.7 (67.1)
2017–2019							
Control	104.6 (4.0)	33.1 (1.6)	5.4 (0.2)	16.2 (11.9)	NA	215.4 (13.2)	760.7 (83.8)
Thinned	53.8 (9.1)	40.5 (2.6)	1.4 (0.2)	16.9 (6.7)	NA	164.0 (13.7)	550.9 (61.8

Standard deviations are in parentheses. All carbon pools are in Mg C ha^{-1} while NPP is in g C m^{-2} yr^{-1}.

Uncertainty estimates in model predictions were quantified using a propagation of error approach that combines the observation uncertainty (i.e., NPP, biomass) with uncertainty in model input parameters and forcing datasets (i.e., climate). Because our climate data was specific to our site for historical simulations, we had no reason to assign any uncertainty for validation with observations. Moreover, because the model was parameterized exclusively with site data, most of our model uncertainty was attributed to variation in our site observations for leaf retention time and belowground biomass.

3. Results

3.1. Pre- and Post-treatment Carbon Stocks (Table 2)

Thinning reduced tree biomass by 47 ± 13% across treatment plots, resulting in a density of 232 ± 23 trees ha^{-1}. Postthinning spacing increased from ~13 to 21 ft (3.3–6.6 m). Residual tree DBH in thinned plots increased from 23 cm prethinning to 27 cm and heights from 14.8 to 16.5 m. Woody debris increased in the thinned plots primarily because of removal operations increased the number of stumps (from ~4.5 to 9.1 Mg C ha^{-1}; Table S1). Thinning reduced understory vegetation biomass by 75%; however, understory vegetation was a minor portion of aboveground live biomass pretreatment (<5%) in all plots. Killed course root mass was the largest source of on-site dead biomass inputs, ranging from 11 to 13 Mg C ha^{-1} per plot. Moderate winter windthrow occurred in treatment plot 6, resulting in 7% mortality of remaining live trees. No additional mortality has been observed in control or treatment plots since observations began in 2016. In total, an estimated 60% of killed aboveground biomass was removed from the site, while most of the remaining portion was piled and burned.

3.2. Net Primary Production

3.2.1. Tree-Level Response to Thinning

In thinned plots, average individual tree NPP increased 70% ± 12% (2017–2019 growth vs. 2012–2016 growth), with the largest increases observed immediately after thinning in 2017 (Figure 2b). In comparison, control plot average tree growth declined by 1%–5% in the same period. Increased average tree growth in thinned plots was a result of both increased growth of remaining individuals (i.e., within-tree NPP increased on average 31% ± 8%) as well as a greater proportion of larger, higher productivity trees. Trees remaining after treatment had been on average 30% more productive and 5 cm larger in DBH than the prethin plot tree average. In remaining trees, there was not a strong relationship between diameter and radial growth ($r = 0.05$). However, consistent radial growth across size classes translated to a geometric positive effect of tree size on volume growth (Figure 2a). Treatment response magnitude and direction was variable; 20% of thinned stand trees did not display increases in radial growth, 50% displayed increases of less than 25%, and 15% of trees displayed increases of over 100% (Figure 2a).

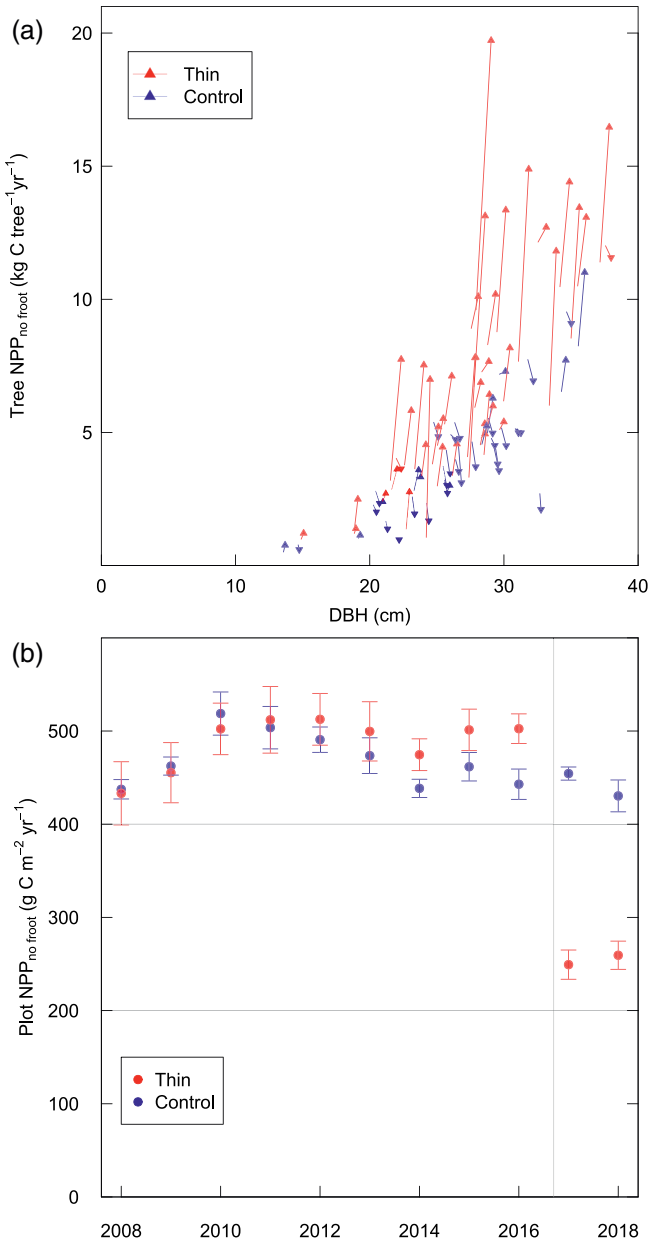

Figure 2. Tree and stand level thinning NPP response. (a) Tree NPP response by DBH. Triangles indicate mean 2017–2018 NPP, triangle direction indicates increases (up) or decreases (down) from the 2015–2016 tree NPP mean, represented by the start of each line. (b**)** Plot level NPP by treatment. Bars indicate SE. Vertical dashed line indicates thinning treatment.

3.2.2. Stand-Level Response to Thinning

At the stand scale, decreases in tree density were not compensated by the increases in tree growth, and NPP decreased by 45% in thinned stands, (-245 ± 23 g C m^{-1} yr^{-1}, $p < 0.05$, paired *T*-test) (Figure 2b). During the same period, control plot NPP declined by 3% (-25 ± 11 g C m^{-1} yr^{-1}). Before treatment, average yearly NPP from 2012 to 2016 across all plots was 790 ± 75 g C m^{-1} yr^{-1}. Through the pretreatment period, NPP sensitivity to yearly climate was relatively low (Figure 2b). NPP excluding fine roots peaked in 2010 (~500 g C m^{-1} yr^{-1}) and declined modestly through 2016, with apparent declines in radial growth approximately balancing increases in tree size and stand biomass. The primary driver of pretreatment stand-level NPP variation was stand age rather than seasonal climate variables (Table S2, LME). Even so, site-wide NPP estimates ranged by only 50 g C m^{-1} yr^{-1} from 2008 to 2016. Though 2015 was an exceptionally hot and dry year, with the longest soil drought period within the observation period, stand NPP nonetheless increased over 2014 (Figure 2b).

Automated dendrometer measurements indicated that stem radial growth occurred from early May until the beginning of August from 2017 to 2019 (Figure 3; ~3 months), a period receiving an average 11% of yearly precipitation during the last decade (2010–2019 Moscow Mountain SNOTEL). Spring rain was not sufficient for preventing continual declines in soil moisture to 30 cm following snow melt (Figure 3). Neither growth start nor end dates varied significantly by treatment ($p < 0.05$, two-sided *t*-tests), despite tree level differences in treatment growth magnitude (Figure 2a). Growth initiation was more rapid (days) than cessation (weeks) and corresponded to the period of soil and air temperature increase immediately after snowmelt. Growth cessation was gradual (approximately the month of July) and corresponded with the depletion of rooting depth VWC. Drought-period circumference shrinkage occurred followed growth cessation and continued until the first major fall rain events, when rapid (i.e., hours to days) circumference recovery occurred upon (Figure 3).

3.3. Respiration

Soil respiration (R_s) between control and treatment plots was similar from weekly to annual time scales (Figure 4), with some seasonal variation. Total annual soil respiration did not significantly vary between treatments during 2018 or 2019 (Table S3 and *t*-test, $p > 0.05$). However, there were periods when control plot means differed from thinned plot means. R_s varied significantly during July and August of 2018 with higher R_s in the thinned stands. Annual R_s ranged from ~830 to 1230 g C m^{-2} yr^{-1} across plots in 2018–2019. Across all years and treatments, concurrent with stem growth, R_s peaked from May through July and declined strongly with declines in VWC from August onwards (LMM; Table S3).

Modeled estimates of component soil respiration fluxes showed a concurrent increase in R_h and decrease in R_a in the thinned plots for several years after thinning, followed by soil R_a recovery and gradual course root decomposition. In both periods, the result was negligible net change in total R_s (Figure S1).

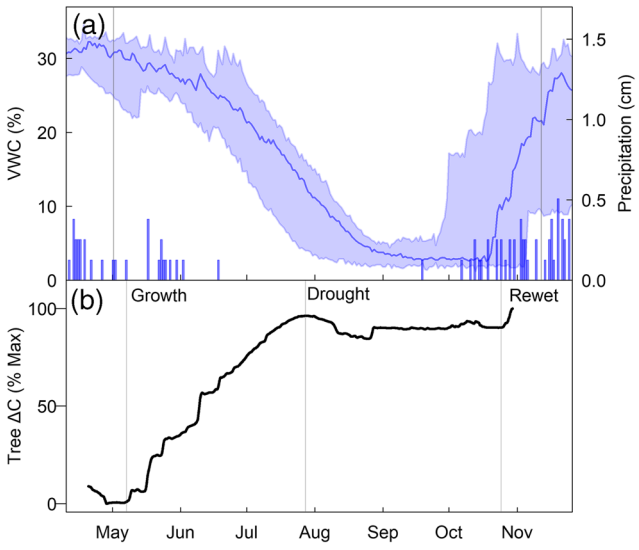

Figure 3. Tree growth and seasonal moisture. (a) 2010–2019 VWC at 20 cm depth (median and range) and daily precipitation (daily median). Vertical gray lines indicate median boundaries of the snow-covered season. Moscow Mountain SNOTEL station. (b) Example dendrometer Δ stem circumference series (ΔC; from early spring minimum) for the study site.

3.4. Sap Flow and Canopy Conductance

3.4.1. Tree-Level Sap Flow and Canopy Conductance

Tree-level sap flow (i.e., at sensor depth) from May-October was 55% and 46% higher in thinned versus control plots in 2018 and 2019, with distinct predrought and drought periods (Figures 5c and 5d, significant treatment effects during all 2018 and 2019 periods, Table S4). In thinned plots, tree sap flow was on average 18% & 26% higher until week 28 in 2018 and week 29 in 2019, when significant drought divergence was observed (Figures 5c and 5d). Spring and early summer sap flow patterns were similar between treatments, with flow under well-hydrated conditions corresponding to variations in temperature and VPD.

Declines in sap flow occurred during rapid soil dry-down (Figure 3) from July through August. While trees in all plots demonstrated declines in sap flow along with declines in site VWC, control-tree flow declined by ~65% from predrought maximum flow by August, while treatment-tree flow declined by ~33%. Continued declines were observed through September, with 87% and 63% decreases for control and treated plots, respectively, relative to mid-season maximums. As a result, tree-level sap flow for trees in the thinned stands from mid-July through October were on average 133% and 90% higher than control stand trees sap flow during 2018 and 2019. For control and thinned plot trees, this drought period represented an average 31%–32% and 40%–48% of measurement period sap flow. Flow past October remained low, though temperatures and VPD declined during this period. During all growing season periods evaluated, treatment and VPD were significant covariates, while VWC was significant across most periods (Table S4).

In 2019, G_c was estimated with the addition of intracanopy temperature and relative humidity measurements. High spring G_c was achieved across treatments by late March to early April, with average daytime G_c 19% higher in thinned stand trees (Figure S1). Daytime G_c for both treatments began to decline sharply in late July (~doy 200) and diverged in magnitude by early August. Thinned stand G_c was on average 165 % higher than in control plots from August through mid-October, with peak differences occurring in early September, after which air temperature and VPD declined through the Fall. During the fall, G_c rose despite consistently low sap flow due to lowered VPD. Spring and Summer $\delta^{13}C$ was also evaluated as a proxy for the intraleaf concentration of CO_2 and intrinsic water use efficiency (i.e., C_i/C_a). Values of $\delta^{13}C$ did not vary significantly between treatments or across the spring and summer drought period ($p < 0.05$, paired and unpaired t-tests).

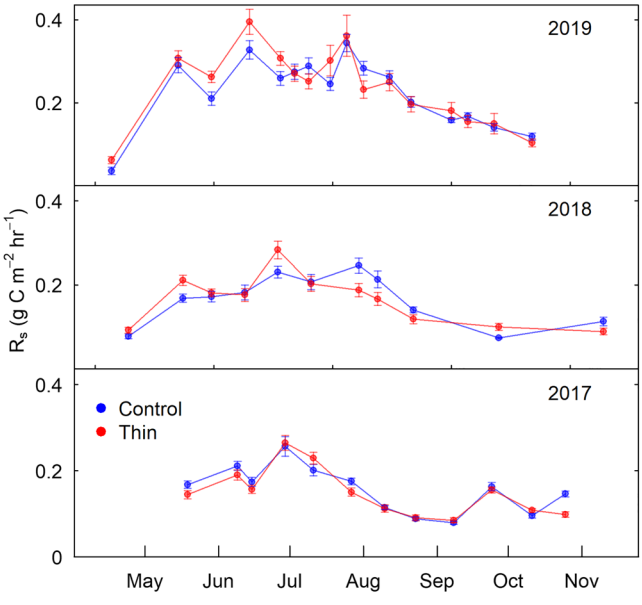

Figure 4. Survey soil respiration observations for control and thinned plots from 2017 to 2019. Error bars represent the standard error for plot-level mean values on each measurement day.

3.4.2. Stand-Level Transpiration

Decreased tree density, sapwood area, and leaf area in the thinned stand (Table 1) resulted in lower stand-level transpiration compared to control plots from May-October (Figures 5a and 5b). Transpiration in the control plots was 74% higher than the thinned plots, varying from 115% higher in early July to 19% more in late October. This difference was greater than 100% in the predrought period, when tree-level sap flow was similar between treatments. In 2018 and 2019, stand-level sap flow approximately converged beginning in August and control stand-level flow decreased below treatment flow in September only (Figures 5a and 5b).

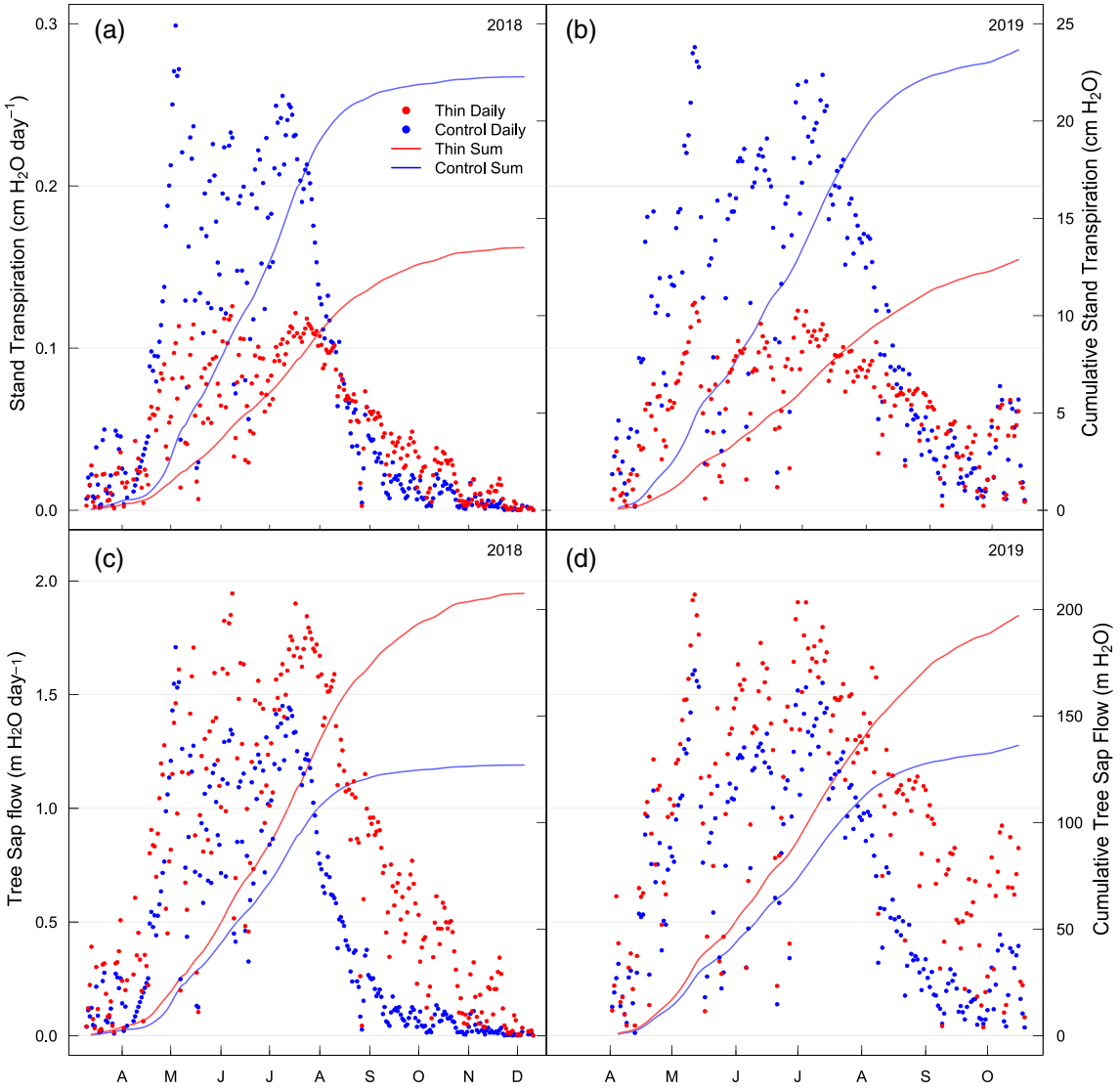

Figure 5. Tree and stand scale sap flow, 2018–2019. (a) Daily and (b) cumulative mean stand transpiration. (c) Daily and (d) cumulative mean tree sap flow.

3.5. Net Forest Carbon Balance (NEP and LCA)

Thinning resulted in an average 48 and 10 Mg C ha^{-1} of killed above and belowground biomass, with 37.4 Mg C ha^{-1} removed from site (Table 1). ~35% of killed biomass remained on site, 18% was combusted as slash or left as debris, and 65% was removed.

Ecosystem partial harvest was simulated in DayCent to investigate trends through 2050 under a warming climate with consistent annual precipitation (Figure S5). Through the observation period, modeled tree component carbon stocks and seasonal patterns of soil moisture driving summer growth cessation compared well to measurements (r^2 = 0.90 and 0.72 respectively. Figures S3 and S4). During the first 5 years postharvest, modeled NEP in thinned stands was lower than control stands, resulting in a maximum posttreatment relative NEP deficit of 12.1 Mg ha^{-1} (Figure 6a). The NEP deficit relative to control stands was overcome by 2035. Low or negative NEP in the first 5 years postharvest resulted from killed belowground biomass decomposition as well as reduced leaf area and NPP (Figure 6a). By 2050, total posttreatment NEP in the thinned stand was 4.6 Mg ha^{-1} higher than control stands, a relative recovery of 16.7 Mg ha^{-1} compared to the posttreatment minimum. Increases in NEP resulted both from increases in NPP and increased allocation to low-turnover wood pools that occurred in part due to increased availability of mineral

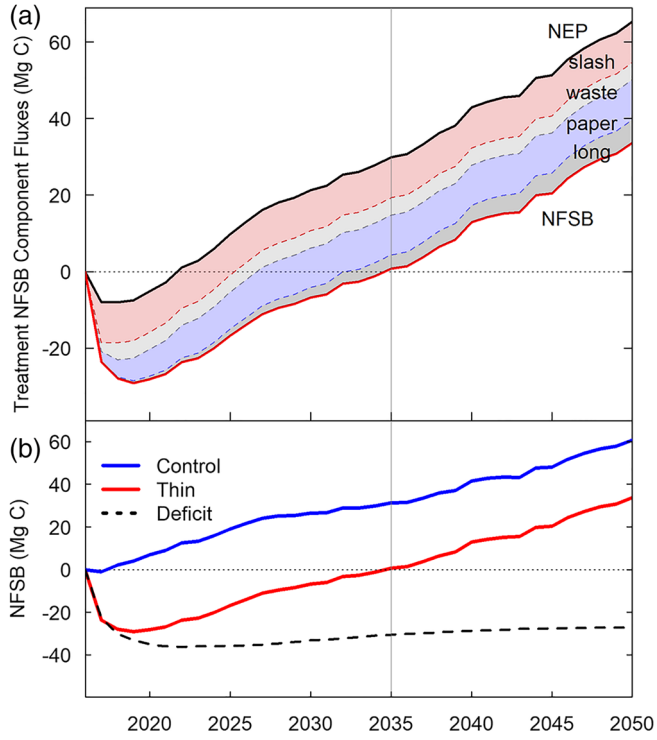

Figure 6. Modeled NFSB post treatment (2017–2050). Vertical gray lines indicate treatment stand recovery to pretreatment total ecosystem carbon stock. (a) Cumulative treatment stand NEP and NFSB and component product emissions. (b) Cumulative treatment and control NFSB. Dotted line indicates thin NFSB deficit relative to control.

nitrogen. Decomposition of killed course roots occurred over several decades and a pulse of postharvest respiration was primarily apparent from the smaller fine root pool. Compared to the control simulation through 2050, differences in stand carbon stocks declined but did not disappear. Aboveground live and total ecosystem carbon in the thinned stand amounted to 75% and 84% of the control in 2050.

Combustion of slash and waste products resulted in 15 Mg C ha^{-1} of harvested biomass emissions within the first 5 years of treatment (Figure 6a). By 2050, 21.0 Mg C ha^{-1} (56%) of removals and 31.6 Mg C ha^{-1} (66%) of killed aboveground biomass had been emitted. Most remaining product carbon remained in long-term pools, which retained 73% (16.4 Mg C ha^{-1}) of inputs in 2050. The NSCB was −26.7 and 33.7 Mg C ha^{-1} in 2021 (5 years) and 2050, representing the net balance of stand-derived carbon both on and off site relative to pretreatment. Thinned stand carbon parity with pretreatment carbon stocks (2016) occurred in less than 20 years. However, the NSCB deficit relative to the control stand was 27.0 Mg C ha^{-1} in 2050, representing the simulated net emissions to the atmosphere relative to control (Figure 6b).

Scenarios with prescribed future mass tree mortality in unthinned stands indicated that most mortality events before 2050 would not exceed the 27.0 Mg C ha^{-1} relative emissions estimated for thinned stands by 2050 (Table S1). Mortality of 50%–95% of tree biomass before 2035 led to control-relative emissions that were 40%–70% of treatment stand relative emissions by 2050. Events of 75%–90% and from ~2035 to 2045 approximately matched or exceeded site 2050 thinning-related relative emissions (maximum increase of 22%). In all cases, while high mortality yielded greater than 40 Mg C ha^{-1} killed biomass, gradual on-site decomposition as well as regrowth or improved residual forest growth led to control-relative 2050 emissions equivalent to less than 25% of killed biomass.

4. Discussion

Forest thinning in a young ponderosa pine plantation resulted in observed and modeled decreases in ecosystem and forest sector carbon storage over unmanaged control plots through the year 2050. Despite increased tree-level production and water use in a location characterized by growing season drought stress, this study affirms inherent site tradeoffs between individual tree vigor and stand carbon storage over time. We estimate that thinned plot carbon stocks will return to prethinned levels by 2035 (Figure 6), but forest sector carbon parity (Mitchell et al., 2012) with untreated plots will not occur by 2050 and therefore represents a relative carbon source to the atmosphere in the absence of disturbance.

After treatment (2017–2019), decreased tree density reduced observed stand biomass and NPP over control (Figure 2b, Table 2), while soil respiration remained similar (Figure 4). Modeled results suggested that thinned stand NEP would exceed control NEP in subsequent years following several years of canopy recovery due to increases in available mineral nitrogen and increased allocation of carbon to wood (and a resulting decrease in biomass turnover). However, a carbon deficit relative to control remained due to the removal of ~40% of live ecosystem carbon as well as the subsequent release of ~60% of removed biomass by 2050. Despite the continued storage of a portion of removed biomass in long-lived wood products, large immediate and short-term emissions were associated with slash combustion, on-site decomposition, and short-term product chain emissions (i.e., waste and paper), and do not represent avoided emissions through 2050. A multidecadal ecosystem biomass (i.e., carbon) deficit following moderate and heavy partial harvest is supported by most analyses of mid to long-term thinning structural impacts (James et al., 2018; Zhou et al., 2013), though we note a general paucity of long-term observations of carbon stocks specific to variable thinning treatments and regions (Williams & Powers, 2019). We highlight that moderate removals

in the productive, even aged study stand (vs. thinning from below, e.g., North & Hurteau, 2011) led to net emissions due to biomass removal and turnover that was rapid relative to yearly ecosystem production (i.e., "slow in, "fast out," Law et al., 2018).

Thinning increased average tree size, diameter growth, and NPP (Figure 2a). Increases in average NPP were a function of both increases in individual tree production as well as altered stand structure (i.e., lower productivity trees being removed; e.g., M. Ryan et al., 1997). A ~70% increase in average tree growth was associated with a more modest ~30% increase in residual tree production. This result highlights the need to differentiate increases in tree production (and, presumably, resilience) from averages that are dependent on structural changes alone when interpreting previous research and anticipating stand and landscape level carbon sequestration and storage (e.g., D'Amato et al., 2013; Sohn et al., 2016; Zhou et al., 2013). Longitudinal observations of individual trees (e.g., Anderson-Teixeira et al., 2015) are generally necessary to isolate tree responses to disturbance and determine the extent to which mean responses are representative of overall stand function and resilience.

Tree growth magnitude within years was not strongly related to growth duration across treatments and individuals, as growth was similarly constrained by mid-summer VPD and VWC (Figure 3). However, thinned plot trees displayed higher sap flow and canopy conductance through the late summer and early fall drought period, implying higher photosynthesis. High-seasonal variability in canopy conductance and a lack of strong variation in C_i/C_a are consistent with conductance as the primary determinant of assimilation in our stands (Drake et al., 2011). These results are also consistent with higher sensitivity of growth (i.e., NPP) than photosynthesis (and GPP) to seasonal moisture stress, a temporary decoupling of carbon supply and carbon demand (Körner, 2003; Muller et al., 2011; Sala et al., 2012), and a likely improved carbon supply of thinned stand trees through the fall and winter. At an individual tree scale, the largest increases in NPP were observed in the growing season immediately after the winter thinning treatment. Though growing seasons 2018–2019 were preceded by markedly improved tree fall and yearly average gas exchange in treatment plots, continued increases in annual stem growth over 2017 were not observed, possibly suggesting altered carbon allocation responses across treatments that were not resolved by our measurements (Körner et al., 2005; M. Ryan et al., 1997).

While observed growing season length and growing season stand water use were similar between treatments, thinned plot trees displayed less severe downregulation of drought-period water use (Figure 5). This implies improved tree carbon and water status during drought moisture stress and winter periods, and the potential for improved resistance to mortality from regional drought or other disturbance (Adams et al., 2017; N. McDowell et al., 2008; Schlesinger et al., 2016; Sevanto et al., 2014). However, the only natural tree mortality observed since 2015 has been mild windthrow in treatment plots. It will be essential to continue current monitoring in orderto observe the long-term impacts of thinning on carbon and water status and how those dynamics effect potential decreases in mortality from disturbance (D'Amato et al., 2013; Sohn et al., 2016; Tepley et al., 2020; van der Molen et al., 2011) that were not prescribed in our modeling. To date, our site observations have been based on treatments in even aged stands of codominant young trees (<40 years). As the stands age, the increased relative size and performance of thinned stand trees (Sohn et al., 2016) may contribute to stand structure that is more resistant to disturbance impacts (Agee & Skinner, 2005). However, forest vulnerability to drought is also complicated by vulnerabilities associated with larger trees that have been related to hydraulic limitations, canopy characteristics, and other factors impacting carbon source strength or sink demand (Bennett et al., 2015; N. G. McDowell & Allen, 2015; Pangle et al., 2015; M. G. Ryan et al., 2006) and can reverse the direction of responses to density as stands age (D'Amato et al., 2013).

Carbon balance tradeoffs between reduced biomass density and increased forest resilience to disturbance are uncertain in large part due to the uncertainty of future natural disturbances occurring in treated areas. Our simulated mass mortality scenarios indicated that 2050 thinning emissions approximately equaled the 2050 emissions from stand mortality events greater than 75% and occurring after 2035. In these experiments, the gradual decomposition of large pools of killed biomass remaining on site highlighted that the emissions consequences of near-term natural disturbances will in part be realized beyond current GHG reduction timelines (e.g., 2035 or 2050, IPCC, 2018). Thus, when managing for forest carbon storage, the timing and magnitude of potential carbon gains or losses, which may be offset in time from disturbance

events, must be considered. In our simulations, the near-parity in carbon emissions from thinning and high natural disturbance late in the simulation period occurred at the stand level. However, at the landscape level, the encounter rates between treatments and disturbance are typically low (J. L. Campbell et al., 2012). Greater areas of forest must therefore be treated than will encounter a disturbance, in turn increasing any carbon cost to benefit ratio estimated at the stand scale. Due to the infeasibility of landscape level treatment experiments, landscape level predictions of disturbance impacts are generally simulated with earth systems models (Buotte, Levis, et al., 2020), which remain limited in their ability to represent stochastic disturbance such as wildfire

Thinning treatment impacts will vary across spatiotemporal scales, meaning our results are both site-specific and have future uncertainty. Furthermore, while our experiment entailed a single thinning intensity, it is possible that lower biomass harvest would have resulted in enhanced residual tree function at lower carbon cost (nonlinear benefits; North & Hurteau, 2011; Zhou et al., 2013). Future work in the region should also better characterize snow accumulation and melt (e.g., SWE) and soil water availability both onsite and at higher elevations to better understand how changes in hydrology will affect thinned and unthinned stands (Krogh et al., 2020).

This study indicated that moderate forest thinning at a northern Rocky Mountain site improved tree function during summer drought at the cost of reduced forest sector carbon balance through 2050. Following treatment, growth and water use increased at the tree scale but decreased at the stand scale due to density reductions. Ecosystem modeling and LCA demonstrated near-term carbon emissions from on and off-site killed biomass that were large relative to annual NPP and therefore unlikely to be overcome in the near-term of GHG mandates (e.g., Hudiburg 2019); this highlights the importance of accounting for the fates of harvested biomass. At a stand level, our results demonstrate that thinning strategies to reduce carbon emissions in the next decades (IPCC, 2018) must either overcome inherent and persistent carbon deficits over nonmanagement or be sufficiently justified for services other than carbon storage (i.e., wood production, human hazard reduction). However, treatments intended to increase carbon storage over business-as-usual should also show that they can do so at the landscape scale and within potentially limited treatment lifetimes (J. L. Campbell et al., 2012). Because the locations of stochastic disturbances (e.g., fire) will occur over only a fraction of a treated area, further landscape (vs. stand) level analyses are ultimately necessary to integrate the prevalence and magnitude of carbon balance impacts from human versus natural disturbances in managed landscapes. It is particularly important to account for region-specific ecosystem carbon density, productivity, and vulnerability to disturbance to establish where treatments may successfully mitigate carbon losses (Buotte, Law, et al., 2020).

Data Availability Statement

The data, model output, and links to model code supporting the conclusions can be obtained in the supporting information and on the Northwest Knowledge Network Repository (https://doi.org/10.7923/0sq1-r267).

Acknowledgments
This work was supported by National Science Foundation award number DEB-1553049. We thank Seth Parker for field data collection and Robert Keefe for providing the harvest operations and advice. The authors declare no competing financial conflicts of interests or other affiliations with conflicts of interest with respect to the results of the paper. Any real or perceived financial conflicts of interests for any author.

References

Abatzoglou, J. T., & Brown, T. J. (2012). A comparison of statistical downscaling methods suited for wildfire applications. *International Journal of Climatology*, *32*(5), 772–780.

Abatzoglou, J. T., & Williams, A. P. (2016). Impact of anthropogenic climate change on wildfire across western US forests. *Proceedings of the National Academy of Sciences*, *113*, 11770–11775. https://doi.org/10.1073/pnas.1607171113

Adams, H. D., Zeppel, M. J., Anderegg, W. R., Hartmann, H., Landhäusser, S. M., Tissue, D. T., et al. (2017). A multi-species synthesis of physiological mechanisms in drought-induced tree mortality. *Nature Ecology and Evolution*, *1*(9), 1285–1291.

Agee, J. K., & Skinner, C. N. (2005). Basic principles of forest fuel reduction treatments. *Forest Ecology and Management*, *211*(1–2), 83–96. https://doi.org/10.1016/j.foreco.2005.01.034

Allen, C. D., Macalady, A. K., Chenchouni, H., Bachelet, D., McDowell, N., Vennetier, M., et al. (2010). A global overview of drought and heat-induced tree mortality reveals emerging climate change risks for forests. *Forest Ecology and Management*, *259*(4), 660–684.

Anderson-Teixeira, K. J., Davies, S. J., Bennett, A. C., Gonzalez-Akre, E. B., Muller-Landau, H. C., Joseph Wright, S., et al. (2015). CTFS-ForestGEO: A worldwide network monitoring forests in an era of global change. *Global Change Biology*, *21*, 528–549. https://doi.org/10.1111/gcb.12712

Bai, E., & Houlton, B. Z. (2009). Coupled isotopic and process-based modeling of gaseous nitrogen losses from tropical rain forests. *Global Biogeochemical Cycles*, *23*, 1–10. https://doi.org/10.1029/2008GB003361

Bartowitz, K. J., Higuera, P. E., Shuman, B. N., McLauchlan, K. K., & Hudiburg, T. W. (2019). Post-Fire Carbon Dynamics in Subalpine Forests of the Rocky Mountains. *Fire*, *2*(4), 58. https://www.mdpi.com/2571-6255/2/4/58

Bates, D., Mächler, M., Bolker, B., & Walker, S. (2014). *Fitting linear mixed-effects models using lme4*. arXiv preprint arXiv:1406.5823.
Bennett, A. C., McDowell, N. G., Allen, C. D., & Anderson-Teixeira, K. J. (2015). Larger trees suffer most during drought in forests worldwide. *Nature Plants*, *1*(10), 15139.
Berner, L. T., Law, B. E., Meddens, A. J. H., & Hicke, J. A. (2017). Tree mortality from fires, bark beetles, and timber harvest during a hot and dry decade in the western United States (2003–2012). *Environmental Research Letters*, *12*(6), 065005. http://stacks.iop.org/1748-9326/12/i=6/a=065005
Brooks, J. R., Meinzer, F. C., Coulombe, R., & Gregg, J. (2002). Hydraulic redistribution of soil water during summer drought in two contrasting Pacific Northwest coniferous forests. *Tree Physiology*, *22*(15–16), 1107–1117. https://doi.org/10.1093/treephys/22.15-16.1107
Brown, R. T., Agee, J. K., & Franklin, J. F. (2004). Forest restoration and fire: principles in the context of place. *Conservation Biology*, *18*(4), 903–912.
Buotte, P. C., Law, B. E., Ripple, W. J., & Berner, L. T. (2020). Carbon sequestration and biodiversity co-benefits of preserving forests in the western United States. *Ecological Applications*, *30*(2), e02039. https://doi.org/10.1002/eap.2039
Buotte, P. C., Levis, S., Law, B. E., Hudiburg, T. W., Rupp, D. E., & Kent, J. J. (2019). Near-future forest vulnerability to drought and fire varies across the western United States. *Global Change Biology*, *25*(1), 290–303.
Campbell, J., Donato, D., Azuma, D., & Law, B. (2007). Pyrogenic carbon emission from a large wildfire in Oregon, United States. *Journal of Geophysical Research: Biogeosciences*, *112*(G4), G04014. https://doi.org/10.1029/2007JG000451
Campbell, J. L., & Ager, A. A. (2013). Forest wildfire, fuel reduction treatments, and landscape carbon stocks: A sensitivity analysis. *Journal of Environmental Management*, *121*, 124–132.
Campbell, J. L., Donato, D. C., & Fontaine, J. B. (2016). Effects of post-fire logging on fuel dynamics in a mixed-conifer forest, Oregon, USA: a 10-year assessment. *International Journal of Wildland Fire*, *25*(6), 646–656. https://doi.org/10.1071/wf15119
Campbell, J. L., Fontaine, J. B., & Donato, D. C. (2016). Carbon emissions from decomposition of fire-killed trees following a large wildfire in Oregon, United States. *Journal of Geophysical Research: Biogeosciences*, *121*, 718–730. https://doi.org/10.1002/2015JG003165
Campbell, J. L., Harmon, M. E., & Mitchell, S. R. (2012). Can fuel-reduction treatments really increase forest carbon storage in the western US by reducing future fire emissions?. *Frontiers in Ecology and the Environment*, *10*, 83–90. https://doi.org/10.1890/110057
Chapin, F., Woodwell, G., Randerson, J., Rastetter, E., Lovett, G., Baldocchi, D., et al. (2006). Reconciling carbon-cycle concepts, terminology, and methods. *Ecosystems*, *9*, 1041–1050. http://dx.doi.org/10.1007/s10021-005-0105-7
Chojnacky, D., Amacher, M., & Gavazzi, M. (2009). Separating duff and litter for improved mass and carbon estimates. *Southern Journal of Applied Forestry*, *33*(1), 29–34.
Ciais, P., Reichstein, M., Viovy, N., Granier, A., Ogee, J., Allard, V., et al. (2005). Europe-wide reduction in primary productivity caused by the heat and drought in 2003. *Nature*, *437*(7058), 529–533. http://www.nature.com/nature/journal/v437/n7058/suppinfo/nature03972_S1.html
D'Amato, A. W., Bradford, J. B., Fraver, S., & Palik, B. J. (2013). Effects of thinning on drought vulnerability and climate response in north temperate forest ecosystems. *Ecological Applications*, *23*(8), 1735–1742.
DellaSala, D. A., Anthony, R. G., Bond, M. L., Fernandez, E. S., Frissell, C. A., Hanson, C. T., & Spivak, R. (2013). Alternative views of a restoration framework for federal forests in the Pacific Northwest. *Journal of Forestry*, *111*(6), 420–429.
Dore, S., Kolb, T. E., Montes-Helu, M., Eckert, S., Sullivan, B., Hungate, B. A., et al. (2010). Carbon and water fluxes from ponderosa pine forests disturbed by wildfire and thinning. *Ecological Applications*, *20*(3), 663–683.
Dore, S., Montes-Helu, M., Hart, S. C., Hungate, B. A., Koch, G. W., Moon, J. B., et al. (2012). Recovery of ponderosa pine ecosystem carbon and water fluxes from thinning and stand-replacing fire. *Global Change Biology*, *18*(10), 3171–3185.
Drake, J. E., Davis, S. C., Raetz, L., & Delucia, E. H. (2011). Mechanisms of age-related changes in forest production: the influence of physiological and successional changes. *Global Change Biology*, *17*(4), 1522–1535.
Dymond, C. C. (2012). Forest carbon in North America: annual storage and emissions from British Columbia's harvest, 1965–2065. *Carbon Balance and Management*, *7*, 8. https://doi.org/10.1186/1750-0680-7-8
Ewers, B. E., Oren, R., Phillips, N., Strömgren, M., & Linder, S. (2001). Mean canopy stomatal conductance responses to water and nutrient availabilities in *Picea abies* and *Pinus taeda*. *Tree Physiology*, *21*(12–13), 841–850.
Farquhar, G. D., Ehleringer, J. R., & Hubick, K. T. (1989). Carbon isotope discrimination and photosynthesis. *Annual Review of Plant Biology*, *40*(1), 503–537.
Fokkema, M., Smits, N., Zeileis, A., Hothorn, T., & Kelderman, H. (2018). Detecting treatment-subgroup interactions in clustered data with generalized linear mixed-effects model trees. *Behavior Research Methods*, *50*(5), 2016–2034. https://doi.org/10.3758/s13428-017-0971-x
Franklin, J. F., Johnson, K. N., & Johnson, D. L. (2018). *Ecological forest management*. Waveland Press.
Goetz, S. J., Bond-Lamberty, B., Law, B. E., Hicke, J. A., Huang, C., Houghton, R. A., et al. (2012). Observations and assessment of forest carbon dynamics following disturbance in North America. *Journal of Geophysical Research*, *117*. https://doi.org/10.1029/2011jg001733
Gomez-Casanovas, N., Anderson-Teixeira, K., Zeri, M., Bernacchi, C. J., & DeLucia, E. H. (2013). Gap filling strategies and error in estimating annual soil respiration. *Global Change Biology*, *19*(6), 1941–1952.
Granier, A., Biron, P., Bréda, N., Pontailler, J. Y., & Saugier, B. (1996). Transpiration of trees and forest stands: short and long-term monitoring using sapflow methods. *Global Change Biology*, *2*(3), 265–274.
Harmon, M. E., Harmon, J. M., Ferrell, W. K., & Brooks, D. (1996). Modeling carbon stores in Oregon and Washington forest products: 1900–1992. *Climatic Change*, *33*(4), 521–550.
Harris, L. B., Scholl, A. E., Young, A. B., Estes, B. L., & Taylor, A. H. (2019). Spatial and temporal dynamics of 20th century carbon storage and emissions after wildfire in an old-growth forest landscape. *Forest Ecology and Management*, *449*, 117461.
Hartman, M. D., Baron, J. S., & Ojima, D. S. (2007). Application of a coupled ecosystem-chemical equilibrium model, DayCent-Chem, to stream and soil chemistry in a Rocky Mountain watershed. *Ecological Modelling*, *200*(3), 493–510.
Hegewisch, K. C., & Abatzoglou, J. T. (2020). Historical climate tracker' web tool. *NW Climate Toolbox*. Retrieved from: https://climatetoolbox.org/
Hicke, J. A., Allen, C. D., Desai, A. R., Dietze, M. C., Hall, R. J., Hogg, E. H., et al. (2012). Effects of biotic disturbances on forest carbon cycling in the United States and Canada. *Global Change Biology*, *18*(1), 7–34. https://doi.org/10.1111/j.1365-2486.2011.02543.x
Hudiburg, T. W., Higuera, P. E., & Hicke, J. A. (2017). Fire-regime variability impacts forest carbon dynamics for centuries to millennia. *Biogeosciences*, *14*(17), 3873–3882. https://doi.org/10.5194/bg-14-3873-2017
Hudiburg, T. W., Law, B. E., Moomaw, W. R., Harmon, M. E., & Stenzel, J. E. (2019). Meeting regional GHG reduction targets requires accounting for all forest sector emissions. *Environmental Research Letters*, *14*(9), 095005.
Hudiburg, T. W., Law, B. E., Wirth, C., & Luyssaert, S. (2011). Regional carbon dioxide implications of forest bioenergy production. *Nature Climate Change*, *1*(8), 419–423. https://doi.org/10.1038/nclimate1264

Hurteau, M., & North, M. (2009). Fuel treatment effects on tree-based forest carbon storage and emissions under modeled wildfire scenarios. *Frontiers in Ecology and the Environment*, *7*(8), 409–414.

Hurteau, M. D., Liang, S., Martin, K. L., North, M. P., Koch, G. W., & Hungate, B. A. (2016). Restoring forest structure and process stabilizes forest carbon in wildfire-prone southwestern ponderosa pine forests. *Ecological Applications*, *26*(2), 382–391.

IPCC. (2018). *Summary for Policymakers. Global warming of 1.5°C*. Geneva, Switzerland:IPCC.

Irvine, J., Law, B., Kurpius, M., Anthoni, P., Moore, D., & Schwarz, P. (2004). Age-related changes in ecosystem structure and function and effects on water and carbon exchange in ponderosa pine. *Tree Physiology*, *24*(7), 753–763.

James, J. N., Kates, N., Kuhn, C. D., Littlefield, C. E., Miller, C. W., Bakker, J. D., et al. (2018). The effects of forest restoration on ecosystem carbon in western North America: A systematic review. *Forest Ecology and Management*, *429*, 625–641.

Katul, G., Lai, C.-T., Schäfer, K., Vidakovic, B., Albertson, J., Ellsworth, D., & Oren, R. (2001). Multiscale analysis of vegetation surface fluxes: from seconds to years. *Advances in Water Resources*, *24*(9–10), 1119–1132.

Katul, G. G., & Albertson, J. D. (1999). Modeling CO_2 sources, sinks, and fluxes within a forest canopy. *Journal of Geophysical Research*, *104*(D6), 6081–6091.

Körner, C. (2003). Carbon limitation in trees. *Journal of Ecology*, *91*(1), 4–17.

Körner, C., Asshoff, R., Bignucolo, O., Hättenschwiler, S., Keel, S. G., Peláez-Riedl, S., et al. (2005). Carbon flux and growth in mature deciduous forest trees exposed to elevated CO_2. *Science*, *309*(5739), 1360–1362.

Krogh, S. A., Broxton, P. D., Manley, P. N., & Harpold, A. A. (2020). Using process based snow modeling and lidar to predict the effects of forest thinning on the Northern Sierra Nevada Snowpack. *Frontiers in Forests and Global Change*, *3*, 21.

Law, B. E., Arkebauer, T., Campbell, J. L., Chen, J., Sun, O., Schwartz, M., et al. (2008). *Terrestrial carbon observations: Protocols for vegetation sampling and data submission*. Rome: FAO.

Law, B. E., Hudiburg, T. W., Berner, L. T., Kent, J. J., Buotte, P. C., & Harmon, M. E. (2018). Land use strategies to mitigate climate change in carbon dense temperate forests. *Proceedings of the National Academy of Sciences*, *115*(14), 201720064.

Law, B. E., Hudiburg, T. W., & Luyssaert, S. (2013). Thinning effects on forest productivity: consequences of preserving old forests and mitigating impacts of fire and drought. *Plant Ecology & Diversity*, *6*(1), 73–85. https://doi.org/10.1080/17550874.2012.679013

Li, Z., Kurz, W. A., Apps, M. J., & Beukema, S. J. (2003). Belowground biomass dynamics in the Carbon Budget Model of the Canadian Forest Sector: recent improvements and implications for the estimation of NPP and NEP. *Canadian Journal of Forest Research*, *33*(1), 126–136.

Liang, S., Hurteau, M. D., & Westerling, A. L. (2018). Large-scale restoration increases carbon stability under projected climate and wildfire regimes. *Frontiers in Ecology and the Environment*, *16*, 207–212. https://doi.org/10.1002/fee.1791

McCauley, L. A., Robles, M. D., Woolley, T., Marshall, R. M., Kretchun, A., & Gori, D. F. (2019). Large-scale forest restoration stabilizes carbon under climate change in Southwest United States. *Ecological Applications*, *29*(8), e01979.

McDowell, N., Pockman, W. T., Allen, C. D., Breshears, D. D., Cobb, N., Kolb, T., et al. (2008). Mechanisms of plant survival and mortality during drought: why do some plants survive while others succumb to drought?. *New Phytologist*, *178*(4), 719–739. https://doi.org/10.1111/j.1469-8137.2008.02436.x

McDowell, N. G., & Allen, C. D. (2015). Darcy's law predicts widespread forest mortality under climate warming. *Nature Climate Change*, *5*(7), 669–672.

Means, J. E., Hansen, H. A., Koerper, G. J., Alaback, P. B., & Klopsch, M. W. (1996). BIOPAK. *The Bulletin of the Ecological Society of America*, *77*(2), 84–85. https://doi.org/10.2307/20168026

Meigs, G., Donato, D., Campbell, J., Martin, J., & Law, B. (2009). Forest fire impacts on carbon uptake, storage, and emission: the role of burn severity in the Eastern Cascades, Oregon. *Ecosystems*, *12*(8), 1246–1267. http://dx.doi.org/10.1007/s10021-009-9285-x

Mitchell, S. R., Harmon, M. E., & O'Connell, K. E. B. (2012). Carbon debt and carbon sequestration parity in forest bioenergy production. *GCB Bioenergy*. http://dx.doi.org/10.1111/j.1757-1707.2012.01173.x

Muller, B., Pantin, F., Génard, M., Turc, O., Freixes, S., Piques, M., & Gibon, Y. (2011). Water deficits uncouple growth from photosynthesis, increase C content, and modify the relationships between C and growth in sink organs. *Journal of Experimental Botany*, *62*(6), 1715–1729.

Naudts, K., Chen, Y., McGrath, M. J., Ryder, J., Valade, A., Otto, J., & Luyssaert, S. (2016). Europe's forest management did not mitigate climate warming. *Science*, *351*(6273), 597–600.

North, M. P., & Hurteau, M. D. (2011). High-severity wildfire effects on carbon stocks and emissions in fuels treated and untreated forest. *Forest Ecology and Management*, *261*(6), 1115–1120.

NRCS. (2010). *Soil survey staff, natural resources conservation service, United States department of agriculture*. Available online at http://soildatamart.nrcs.usda.gov

Pangle, R., Kavanagh, K., & Duursma, R. (2015). Decline in canopy gas exchange with increasing tree height, atmospheric evaporative demand, and seasonal drought in co-occurring inland Pacific Northwest conifer species. *Canadian Journal of Forest Research*, *45*(8), 1086–1101.

Parton, W. J., Hartman, M., Ojima, D., & Schimel, D. (1998). DAYCENT and its land surface submodel: Description and testing. *Global and Planetary Change*, *19*(1–4), 35–48. https://doi.org/10.1016/s0921-8181(98)00040-x

Reichstein, M., Rey, A., Freibauer, A., Tenhunen, J., Valentini, R., Banza, J., et al. (2003). Modeling temporal and large-scale spatial variability of soil respiration from soil water availability, temperature and vegetation productivity indices. *Global Biogeochemical Cycles*, *17*(4), 1104. https://doi.org/10.1029/2003GB002035,4

Ryan, M., Binkley, D., & Fownes, J. H. (1997). Age-related decline in forest productivity: Pattern and process. In M. Begon & A. H. Fitter (Eds.), *Advances in Ecological Research* (pp. 213–262). Elsevier. https://www.sciencedirect.com/science/article/pii/S006525040860001X

Ryan, M. G., Phillips, N., & Bond, B. J. (2006). The hydraulic limitation hypothesis revisited. *Plant, Cell and Environment*, *29*(3), 367–381. https://doi.org/10.1111/j.1365-3040.2005.01478.x

Sala, A., Woodruff, D. R., & Meinzer, F. C. (2012). Carbon dynamics in trees: Feast or famine?. *Tree Physiology*, *32*(6), 764–775.

Schaefer, G. L., & Paetzold, R. F. (2001). SNOTEL (SNOwpack TELemetry) and SCAN (soil climate analysis network). In *Paper presented at the Proceeding of International Workshop on Automated Wea. Stations for Applications in Agr. and Water Resource Management*.

Schlesinger, W. H., Dietze, M. C., Jackson, R. B., Phillips, R. P., Rhoades, C. C., Rustad, L. E., & Vose, J. M. (2016). Forest biogeochemistry in response to drought. *Global Change Biology*, *22*(7), 2318–2328.

Schwalm, C. R., Williams, C. A., Schaefer, K., Anderson, R., Arain, M. A., Baker, I., et al. (2010). A model-data intercomparison of CO_2 exchange across North America: Results from the North American Carbon Program site synthesis. *Journal of Geophysical Research*, *115*(G3), G00H05. https://doi.org/10.1029/2009JG001229

Schwalm, C. R., Williams, C. A., Schaefer, K., Baldocchi, D., Black, T. A., Goldstein, A. H., et al. (2012). Reduction in carbon uptake during turn of the century drought in western North America. *Nature Geoscience*, *5*(8), 551–556.

Sevanto, S., Mcdowell, N. G., Dickman, L. T., Pangle, R., & Pockman, W. T. (2014). How do trees die? A test of the hydraulic failure and carbon starvation hypotheses. *Plant Cell and Environment*, *37*(1), 153–161.

Skog, K. E. (2008). Sequestration of carbon in harvested wood products for the United States. *Forest Products Journal*, Vol. *58*(6), 56–72.

Smith, J. E., Heath, L., Skog, K. E., & Birdsey, R. (2006). *Methods for calculating forest ecosystem and harvested carbon with standard estimates for forest types of the United States gen. Tech. Rep. NE-343*. PA: Newtown Square.

Sohn, J. A., Saha, S., & Bauhus, J. (2016). Potential of forest thinning to mitigate drought stress: A meta-analysis. *Forest Ecology and Management*, *380*, 261–273.

State of California Executive Department. (2018). Sacremento, CA. Retrieved from https://www.gov.ca.gov/wp-content/uploads/2018/05/5.10.18-Forest-EO.pdf

Stenzel, J. E., Bartowitz, K. J., Hartman, M. D., Lutz, J. A., Kolden, C. A., Smith, A. M. S., et al. (2019). Fixing a snag in carbon emissions estimates from wildfires. *Global Change Biology*, *25*. https://doi.org/10.1111/gcb.14716

Tague, C. L., Moritz, M., & Hanan, E. (2019). The changing water cycle: The eco-hydrologic impacts of forest density reduction in Mediterranean (seasonally dry) regions. *WIREs Water*, *6*(4), e1350. https://doi.org/10.1002/wat2.1350

Tepley, A. J., Hood, S. M., Keyes, C. R., & Sala, A. (2020). Forest restoration treatments in a ponderosa pine forest enhance physiological activity and growth under climatic stress. *Ecological Applications*, *30*, e02188. https://doi.org/10.1002/EAP.2188

Thornton, P., Thornton, M. N. W., Wei, Y., & Cook, R. B. (2012). *Daymet: Daily surface weather on a 1 km grid for North America, 1980 - 2008*. WOS:000319907800016

Tsamir, M., Gottlieb, S., Preisler, Y., Rotenberg, E., Tatarinov, F., Yakir, D., et al. (2019). Stand density effects on carbon and water fluxes in a semi-arid forest, from leaf to stand-scale. *Forest Ecology and Management*, *453*, 117573.

U.S. Executive Office of the President. (2018). *Promoting Active Management of America's Forests, Rangelands, and Other Federal Lands To Improve Conditions and Reduce Wildfire Risk (Executive Order 13855)*. Washington, DC.

van der Molen, M. K., Dolman, A. J., Ciais, P., Eglin, T., Gobron, N., Law, B. E., et al. (2011). Drought and ecosystem carbon cycling. *Agricultural and Forest Meteorology*, *151*(7), 765–773. https://doi.org/10.1016/j.agrformet.2011.01.018

Van Wagner, C. E. (1968). The line-intersect method in furest fuel sampling. *Forest Science*, *14*, 20–26.

Varhola, A., Coops, N. C., Weiler, M., & Moore, R. D. (2010). Forest canopy effects on snow accumulation and ablation: An integrative review of empirical results. *Journal of Hydrology*, *392*(3–4), 219–233.

Wanek, W., Heintel, S., & Richter, A. (2001). Preparation of starch and other carbon fractions from higher plant leaves for stable carbon isotope analysis. *Rapid Communications in Mass Spectrometry*, *15*(14), 1136–1140.

Ward, E. J., Domec, J.-C., King, J., Sun, G., McNulty, S., & Noormets, A. (2017). TRACC: An open source software for processing sap flux data from thermal dissipation probes. *Trees*, *31*(5), 1737–1742.

Williams, N. G., & Powers, M. D. (2019). Carbon storage implications of active management in mature *Pseudotsuga menziesii* forests of western Oregon. *Forest Ecology and Management*, *432*, 761–775.

Zeileis, A., Hothorn, T., & Hornik, K. (2008). Model-based recursive partitioning. *Journal of Computational & Graphical Statistics*, *17*(2), 492–514.

Zhao, M., & Running, S. W. (2010). Drought-induced reduction in global terrestrial net primary production from 2000 through 2009. *Science*, *329*(5994), 940–943.

Zhou, D., Zhao, S., Liu, S., & Oeding, J. (2013). A meta-analysis on the impacts of partial cutting on forest structure and carbon storage. *Biogeosciences*, *10*(6), 3691–3703.